Localized modes in $\chi^{(2)}$ media with $\mathcal{PT}$-symmetric localized potential

F. C. Moreira,[1,2] F. Kh. Abdullaev,[3] V. V. Konotop,[2] and A. V. Yulin[2]

[1]*Universidade Federal de Alagoas, Campus A. C. Simões, Avenida Lourival Melo Mota, s/n, Cidade Universitária, Maceió Alagoas 57072-900, Brazil*

[2]*Departamento de Física, Centro de Física Teórica e Computacional, Faculdade de Ciências, Universidade de Lisboa, Avenida Professor Gama Pinto 2, Lisboa 1649-003, Portugal*

[3]*Instituto de Fisica Teórica, Universidade Estadual Paulista, Rua Dr. Bento Teobaldo Ferraz, 271 Barra Funda, São Paulo, Código de Endereçamento Postal 01140-070, Brazil*

(Received 14 September 2012; revised manuscript received 11 October 2012; published 15 November 2012)

We study the existence and stability of solitons in the quadratic nonlinear media with spatially localized parity-time- ($\mathcal{PT}$)-symmetric modulation of the linear refractive index. Families of stable one- and two-hump solitons are found. The properties of nonlinear modes bifurcating from a linear limit of small fundamental harmonic fields are investigated. It is shown that the fundamental branch, bifurcating from the linear mode of the fundamental harmonic is limited in power. The power maximum decreases with the strength of the imaginary part of the refractive index. The modes bifurcating from the linear mode of the second harmonic can exist even above the $\mathcal{PT}$-symmetry-breaking threshold. We found that the fundamental branch bifurcating from the linear limit can undergo a secondary bifurcation colliding with a branch of two-hump soliton solutions. The stability intervals for different values of the propagation constant and gain or loss gradient are obtained. The examples of dynamics and excitations of solitons obtained by numerical simulations are also given.

DOI: 10.1103/PhysRevA.86.053815 PACS number(s): 42.65.Tg, 42.65.Sf

I. INTRODUCTION

Non-Hermitian Hamiltonians satisfying the parity-time ($\mathcal{PT}$) symmetry can have real eigenvalues [1]. Although these ideas were originally developed in the quantum-mechanical context, it soon became clear that new broad applications could be found in optics. The first suggestions of the optical analogs of the $\mathcal{PT}$-symmetric Hamiltonians were proposed in Ref. [2] and were based on a linear planar waveguide structure. $\mathcal{PT}$-symmetry effect predictions are confirmed in experiments with light propagation in couplers with gains and losses [3]. Later on, exploring nonlinear optical media obeying $\mathcal{PT}$ symmetry was suggested, and, in particular, the possibility for soliton propagation was shown in such media [4]. The $\mathcal{PT}$ symmetry was modeled by the refractive index having a symmetric real part and an antisymmetric imaginary part. A particularly interesting realization of a $\mathcal{PT}$-symmetric modulation of the refractive index is when losses and gains are localized in space, giving rise to a $\mathcal{PT}$-symmetric localized impurity. Such impurities allow for the existence of localized (defect) modes. In the linear theory, in Refs. [5,6], such modes were studied for exactly integrable models, and their nonlinear extension was reported in Ref. [4]. Solitons supported by other $\mathcal{PT}$-symmetric defects were also reported for focusing [7] and defocusing [8] media. Linear scattering by a $\mathcal{PT}$-symmetric inhomogeneity and the emergence of the related spectral singularities were described in Ref. [9]. The effect of two and various randomly distributed $\mathcal{PT}$-symmetric impurities on the lattice dynamics was addressed in Ref. [10]. Switching of solitons in a unidirectional coupler using $\mathcal{PT}$-symmetric defects was suggested in Ref. [11]. Nonlinear modes in even more sophisticated double-well $\mathcal{PT}$-symmetric potentials were studied recently [12].

All of the papers mentioned above and devoted to nonlinear modes dealt with the $\mathcal{PT}$-symmetric media possessing Kerr nonlinearity (see the list of recent papers on solitons in Ref. [13]). Furthermore, it is a natural step to address the possibility of the existence of defect modes and their stability in another class of widely used optical media, which is the $\chi^{(2)}$ materials. Solitons in quadratic nonlinear media with conservative defects were investigated in Refs. [14,15] where it was shown that solutions were dynamically stable in the case of attractive impurities. In the present paper, we study the existence of solitons in the media with quadratic nonlinearity and localized $\mathcal{PT}$-symmetric potentials.

The paper is organized as follows. In Sec. II, the model and statement of the problem are formulated. The properties of localized modes for different ratios between fundamental and second harmonics are studied in Secs. III–V. The stability and dynamics of localized solutions are considered in Sec. VI.

II. STATEMENT OF THE PROBLEM

We consider the system,

$$i\frac{\partial u_1}{\partial \zeta}+\frac{\partial^2 u_1}{\partial \xi^2}+V\left(\frac{1}{\cosh^2\xi}+i\alpha\frac{\sinh\xi}{\cosh^2\xi}\right)u_1+2\bar{u}_1u_2=0, \tag{1a}$$

$$i\frac{\partial u_2}{\partial \zeta}+\frac{1}{2}\frac{\partial^2 u_2}{\partial \xi^2}+2\left(\frac{V}{\cosh^2\xi}+q\right)u_2+u_1^2=0, \tag{1b}$$

describing spatial second-harmonic generation in a $\chi^{(2)}$ material with localized modulation of the refractive index, u_1 and u_2 being the dimensionless fields of the first and second harmonics, ξ and ζ are the dimensionless transverse and propagation coordinates, scaled to the characteristic size of the modulation of the refractive index, which is characterized by the amplitude V. The mismatch in the propagation constants of field components is described by q. We notice that, experimentally, the introduced model can describe a medium

with active dopants, typically having rather narrow spectral resonances, i.e., affecting only a limited range of frequencies. In particular, such impurities can induce gain and dissipation, whose strengths are characterized by α only for one of the field components, which, in our case, is the Fundamental Field (FF).

Before getting into the detailed study of the system (1), we note that, in the standard way, solitonic solutions can be found in the analytical form in the limit of large mismatch parameter $-q \gg 1$ when $u_2 \approx -u_1^2/(2q)$, and the system (1) reduces to the nonlinear Schrödinger equation with the $\mathcal{PT}$-symmetric potential for the fundamental harmonic u_1,

$$i\frac{\partial u_1}{\partial \zeta} + \frac{\partial^2 u_1}{\partial \xi^2} + V\left(\frac{1}{\cosh^2\xi} + i\alpha\frac{\sinh\xi}{\cosh^2\xi}\right) - \frac{1}{q}|u_1|^2 u_1 = 0. \tag{2}$$

For $q < 0$, the bright soliton solution has the form Ref. [4]

$$u_1 = \sqrt{|q|A}\,\mathrm{sech}(\xi)\exp\left[i\frac{\alpha V}{3}\tan^{-1}[\sinh(\xi)] + i\zeta\right], \qquad A = \left(2 - V + \frac{\alpha^2 V^2}{9}\right). \tag{3}$$

We are interested in the localized solutions,

$$u_n(\xi,\zeta) = w_n(\xi)e^{inb\zeta}, \qquad n = 1,2, \tag{4}$$

where b is the propagation constant of the first harmonic and $w_{1,2}$ solves the system,

$$\frac{d^2 w_1}{d\xi^2} + \left[V\left(\frac{1}{\cosh^2\xi} + i\alpha\frac{\sinh\xi}{\cosh^2\xi}\right) - b\right]w_1 + 2\overline{w}_1 w_2 = 0, \tag{5a}$$

$$\frac{1}{2}\frac{d^2 w_2}{d\xi^2} + 2\left(V\frac{1}{\cosh^2\xi} + q - b\right)w_2 + w_1^2 = 0 \tag{5b}$$

subject to the zero boundary conditions $w_{1,2}(\xi) \to 0$ as $|\xi| \to \infty$.

We restrict our consideration mainly to solutions bifurcating from the linear limit, which is understood as a limit where, at least, one of the harmonics vanishes. It follows from Eqs. (1), that the so-defined linear limit does not necessarily imply that both amplitudes w_1 and w_2 are infinitely small. Indeed, it is sufficient to require that only the amplitude of the fundamental harmonic w_1 is infinitely small to consider Eqs. (1) in the linear limit. That is why one can distinguish three different bifurcations of the fundamental soliton solution from the linear limit:

(i) The amplitude of the second harmonic is on the order of the squared amplitude of the first harmonic, i.e., is negligible compared to the amplitude of the first harmonic,

$$w_2 = O\left(w_1^2\right), \quad w_1 \to 0. \tag{6}$$

(ii) The second harmonic is finite in the limit of the negligible first harmonic,

$$w_2 = O(1), \quad w_1 \to 0. \tag{7}$$

(iii) Both harmonics are on the same order,

$$w_2 = O(w_1), \qquad w_1 \to 0. \tag{8}$$

As follows from Eqs. (6) and (8), the maximal intensities of both w_1 and w_2 go to zero at the bifurcation point for cases (i) and (iii). However, in case (ii), the maximum of the absolute value of field w_2 goes to a finite value when the solution approaches the bifurcation point. Which of the cases is realized depends on the parameters of the system and, in particular, on the mismatch q. Below, we consider these three cases separately.

III. MODES WITH NEGLIGIBLE SECOND HARMONICS IN THE LINEAR LIMIT

Let us start with the conditions necessary for Eq. (6) to occur. In this limit, the nonlinear term in Eq. (5a) can be neglected, and in the leading order, we have the eigenvalue problem,

$$L_{1,\alpha} w_{1l} = b w_{1l}, \tag{9a}$$

$$L_{1,\alpha} = \frac{d^2}{d\xi^2} + V\left(\frac{1}{\cosh^2\xi} + i\alpha\frac{\sinh\xi}{\cosh^2\xi}\right). \tag{9b}$$

Equation (9) has been studied before. Therefore, below, we only briefly outline the features necessary for our analysis, referring to Refs. [5,6] for more details.

For $V > 0$, Eq. (9) possesses localized solutions. When α is below the $\mathcal{PT}$-symmetry-breaking threshold,

$$\alpha < \alpha_{cr} = 1 + \frac{1}{4V}, \tag{10}$$

the spectrum of Eq. (9) has discrete real eigenvalues given by Ref. [16]

$$b_{1,n} = (n - \eta_1)^2, \qquad n = 0,1,\ldots < \eta_1, \tag{11}$$

where

$$\eta_1 = \tfrac{1}{2}\left(\sqrt{V(\alpha_{cr} - \alpha)} + \sqrt{V(\alpha + \alpha_{cr})} - 1\right). \tag{12}$$

Above the symmetry-breaking point ($\alpha > \alpha_{cr}$), the eigenvalues of the bound states are complex valued. We notice here that no fundamental branch, satisfying condition (6) with $\alpha > \alpha_{cr}$, was found.

Therefore, from now on, we concentrate only on the results for $\mathcal{PT}$-symmetry preserving case (10). Moreover, our consideration will be limited to nonlinear modes that bifurcate from the ground state of the defect potential in Eq. (9), i.e., $n = 0$. The respective eigenstate of the linear problem (9) reads [5,6]

$$w_{1l}(\xi) = W_1\,\mathrm{sech}^{\eta_1}(\xi)\exp\left[\frac{i}{2}\Theta\,\tan^{-1}(\sinh\xi)\right], \tag{13}$$

where W_1 is a constant and

$$\Theta = \sqrt{V(\alpha_{cr} - \alpha)} - \sqrt{V(\alpha + \alpha_{cr})}. \tag{14}$$

Passing to Eq. (5b), in the small amplitude limit, one can look for a solution with $w_1 \approx w_{1l}$, which plays the role of the inhomogeneous term in the linear equation for w_2. However, to obtain the complete families of solutions, one has to consider both Eqs. (1). We did this using the relaxation Newton-Raphson method using the described linear solutions as the initial ansatz.

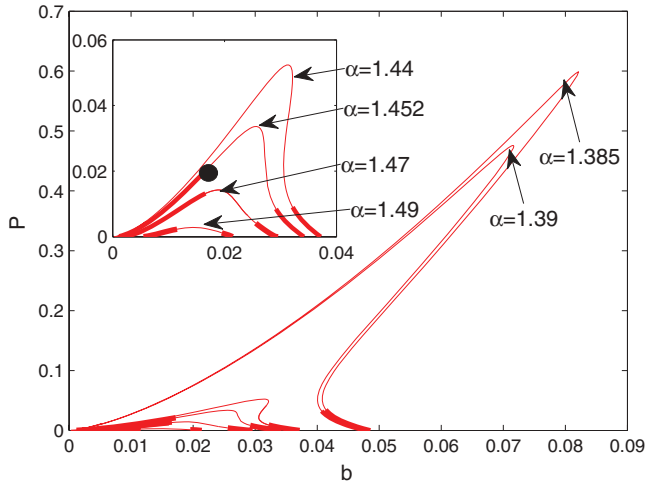

FIG. 1. (Color online) Families of the solutions bifurcating from $b_{1,0} = \eta_1^2$ in case (i) for several values of α. Thick (thin) lines represent stable (unstable) solutions. The inset shows the branches for larger values of α. The black circles represent solutions studied in the text. The parameters of the structure are $V = 1/2$, $q = 0$, and $\alpha_{cr} = 1.5$.

Figure 1 shows the dependence of the total power,

$$P = P_1 + P_2, \qquad P_n = n \int_{-\infty}^{\infty} |w_n|^2 d\xi, \tag{15}$$

on the propagation constant with several values of α. We observe that the fundamental branches shown in Fig. 1 have a maximal in power P_M, $P \leqslant P_M$. The value of P_M is decreasing as α increases. We also observed that $P_M \to 0$ as $\alpha \to \alpha_{cr}$, i.e., the fundamental branch disappears. For a given α, the position of P_M with respect to b approaches $b = 0$ as q decreases as one can see in Fig. 2. The position of P_M moves to the right in the case of $q > 0$. In Fig. 2, one can also see that, in this case, the branch ends in $b = -q$ because the mismatch shifts the position of the continuum spectrum of the linear part of Eq. (5b) and w_2 becomes delocalized. There is no low amplitude linear limit for w_1 in this case.

In Fig. 3, we show the typical distributions of the fields w_n and the real-valued currents j_n defined as ($n = 1,2$)

$$j_n(\xi) = |w_n|^2 \frac{d\theta_n}{d\xi}, \quad \theta_n(\xi) = \arg w_n(\xi). \tag{16}$$

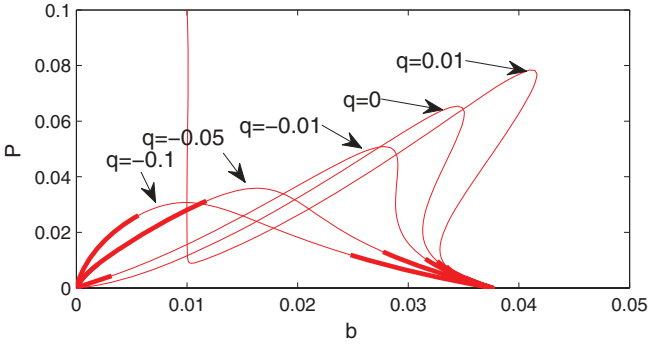

FIG. 2. (Color online) Families of the solutions bifurcating from $b_{1,0} = \eta_1^2$ and corresponding to case (i) for several values of q. Thick (thin) lines represent stable (unstable) solutions. The parameters of the structure are $V = 1/2$ and $\alpha = 1.44$.

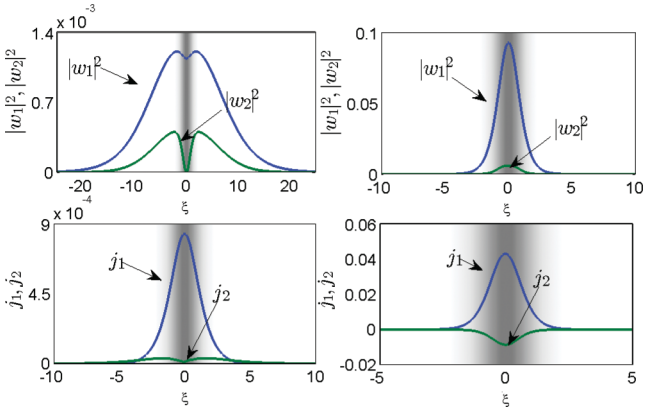

FIG. 3. (Color online) Upper panels: Spatial distributions of the intensities $|w_n|^2$ and lower panels: the currents j_n. The left panels correspond to a stable solution with $b = 0.024$ as marked by a black circle in Fig. 1, pertaining to the fundamental branch that bifurcates from $b_{1,0} = 0.034$ where $V = 1/2$, $q = 0$, and $\alpha = 1.452$. The right panels correspond to a stable solution with $b = 0.82$, pertaining to the fundamental branch that bifurcates from $b_{1,0} = 0.92$ where $V = 2$, $q = 0$, and $\alpha = 0.5$. Shadowed domains show the localized impurity (darker areas represent higher values of its real part $V\,\mathrm{sech}^2\xi$.

By construction, $|w_n|^2$ and j_n are even functions. The effective width of the intensities of modes may significantly exceed the size of the impurity, particularly, in the modes closer to the edge of the continuous spectrum (the left panels of Fig. 3).

We note that, in the left panels of Fig. 3, the solution has a relatively small amplitude. This is a peculiarity of the chosen strength of the potential (it was $V = 1/2$, solitons with larger amplitudes were be found to be unstable). Although this potential (ensuring the existence of only one linear defect level in the localized potential) is used below in the text, in the right panels of Fig. 3, we show a higher amplitude soliton for the potential well having the width $V = 2$ (and the parameters $\alpha = 0.5$ and $q = 0$).

IV. NONLINEAR MODES WITHOUT LINEAR LIMITS

In this section, we investigate the case when the second harmonic remains finite at $w_1 \to 0$. Then, one can neglect the nonlinear term w_1^2 in Eq. (5b) reducing it to the well-known

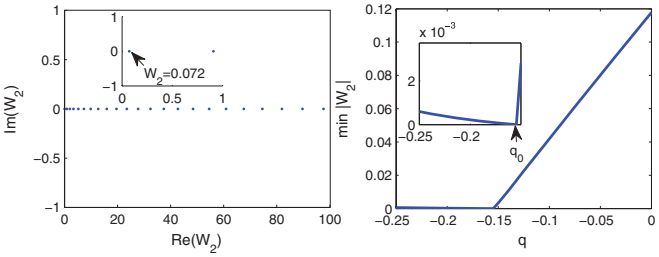

FIG. 4. (Color online) Left panel: The eigenvalues W_2 of Eq. (17). The parameters of the structure are $V = 1/2$, $\alpha = 1.4$, and $q = 0$. The inset shows the first few eigenvalues in detail. Right panel: The lowest $|W_2|$ of Eq. (17) as a function of the mismatch q of the lowest P branch. The inset shows how the minimum value of W_2 reaches zero at $q = q_0$.

linear eigenvalue problem (see, e.g., Ref. [17]),

$$L_2 w_{2l} = 2b w_{2l}, \tag{17a}$$

$$L_2 = \frac{1}{2}\frac{d^2}{d\xi^2} + 2\left(V\frac{1}{\cosh^2\xi} + q\right), \tag{17b}$$

whose eigenvalues are

$$b_{2,n} = \frac{(n-\eta_2)^2}{4} + q, \quad n < 0,1,\ldots, \quad \eta_2 = \sqrt{\frac{1}{4}+4V} - \frac{1}{2}. \tag{18}$$

Here, we again consider the case where there is only one localized mode. This leads to the requirement that $\eta_2 \leqslant 1$ and, consequently, $V \leqslant 1/2$. The corresponding eigenfunction of $b_{2,0}$ reads

$$w_{2,0}(\xi) = W_2 \mathrm{sech}^{\eta_2}\xi, \tag{19}$$

where W_2 is some constant which must be determined. This can be performed from the condition that the propagation constants in Eqs. (5a) and (17) are the same. In the vicinity of the bifurcation point, one can approximate $w_2 \approx w_{2l}$, i.e., Eq. (5a) can be approximated by the following linear system:

$$L\begin{pmatrix}\bar{w}_1\\ w_1\end{pmatrix} = W_2\begin{pmatrix}\bar{w}_1\\ w_1\end{pmatrix}, \tag{20a}$$

$$L = -\frac{1}{2}\cosh^{\eta_2}(\xi)\begin{pmatrix}0 & L_1 - b_{2,0}\\ \bar{L}_1 - b_{2,0} & 0\end{pmatrix}. \tag{20b}$$

Let us note that (20b) is an eigenvalue equation, and so, the allowed values of W_2 are simply the eigenvalues. Next, we define bra and ket vectors: $\langle\psi| \equiv (\psi(\xi), \bar{\psi}(\xi))$ and $|\psi\rangle \equiv (\bar{\psi}(\xi), \psi(\xi))^T$ (T stays for the transpose matrix), where $\psi(\xi) \to 0$ at $\xi \to \pm\infty$ and verify that the operator L is Hermitian with respect to the weighted inner product,

$$\langle\psi_1|\psi_2\rangle = \int_{-\infty}^{\infty} \mathrm{sech}^{\eta_2}(\xi)[\psi_1(\xi)\bar{\psi}_2(\xi) + \bar{\psi}_1(\xi)\psi_2(\xi)]d\xi. \tag{21}$$

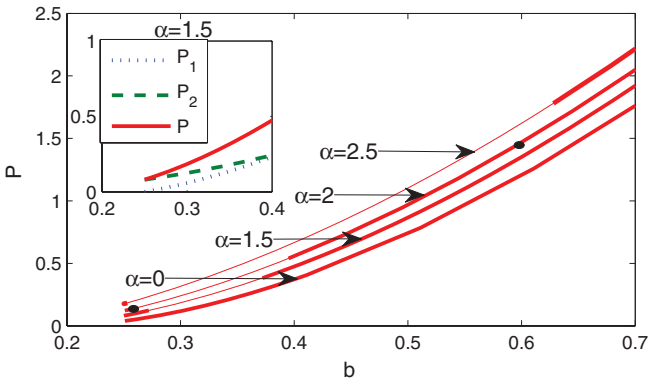

FIG. 5. (Color online) The power diagrams of the fundamental branches bifurcating from the linear mode $b_{2,0} = 0.25$ for several values of α. Thick (thin) lines represent stable (unstable) solutions. The inset shows, in detail, that P_1 goes to zero in the vicinity of $b_{2,0}$, whereas, P_2 remains finite. Filled circles represent two stable solutions shown below in Fig. 6. The parameters of the structure are $V = 1/2$ and $q = 0$.

The Hermiticity of L ensures the reality of the admissible W_2. We also note that, if $(\bar{w}_1(\xi), w_1(\xi))^T$ is a solution of Eq. (17) with eigenvalue W_2, then $-W_2$ is also an eigenvalue with eigenfunction $(-i\bar{w}_1(\xi), iw_1(\xi))^T$. This allows us to restrict the consideration to $W_2 > 0$.

We investigated the system (17) numerically and found that there is an infinite number of discrete eigenvalues W_2. The ones having the smallest absolute values are shown in Fig. 4. The amplitude of the second harmonic W_2 depends on $b = b_{2,0}$ [see Eq. (20b)]. In Fig. 4, we show the dependence of W_2 on q corresponding to the lowest $|W_2|$ branch. The special case when, for a certain value of q, the amplitude of the second harmonic $W_2 \to 0$ happens when $b_{1,0} = b_{2,0}$. This leads to

$$q = q_0, \qquad q_0 = \eta_1^2 - \tfrac{1}{4}\eta_2^2, \tag{22}$$

which is precisely the case, however, (8); we consider it in the next section.

We numerically studied the existence of bifurcations satisfying (7) in Fig. 5. It is possible to see, in the inset of Fig. 5, that, at the bifurcation point, the branches satisfy $P_1(b_{2,0}) = 0$ and, consequently, $P(b_{2,0}) = P_2(b_{2,0})$. A simple integration in (15) after the substitution $w_2 = w_{2l}$ reveals that, for each α when $V = 1/2$ and $\eta_2 = 1$ (the case of Fig. 5), one has $P(b_{2,0}) = 4W_2^2$.

It can be seen in Fig. 5 for the power diagrams of the fundamental branches where stable solutions exist above the $\mathcal{PT}$-symmetry-breaking point. The existence of stable nonlinear modes, even when the spectrum of the linear system is not purely real, has been reported earlier in Ref. [18] (see also recent paper [19]).

In Fig. 6, there is an example of a mode in case (ii).

V. BIFURCATION OF THE NONLINEAR MODES FROM THE LINEAR SPECTRUM

Now, we consider case (iii) for which the relation (8) holds. Previously, we have shown that, if the bifurcation point is, at the same time, an eigenvalue of Eq. (9) and (17), i.e., $b_{1,0} = b_{2,0}$, then the mismatch must have the special value $q = q_0$. We also have seen that, in this case, $W_2 = 0$. As a direct consequence, (17) reduces to Eq. (9) and not only $w_2 \to w_{2l}$, but also the FFs satisfy $w_1 \to w_{1l}$ at the bifurcation point.

Figure 7 shows power diagrams of solutions satisfying (8) for several values of α. It is possible to see that two bifurcations occur at $b = b_{1,0} = b_{2,0}$ (see the dashed line in the inset of Fig. 7). The branch that goes to the right is a bifurcation of

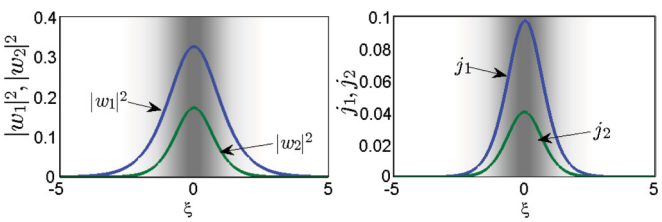

FIG. 6. (Color online) An example of a stable solution of case (ii) with $b = 0.6$ and $\alpha = 2 > \alpha_{cr}$, marked with the filled circle in Fig. 5. Shadowed domains show the localized impurity (darker areas representing higher values of the real part of the localized potential). The parameters of the structure are $V = 1/2$ and $q = 0$.

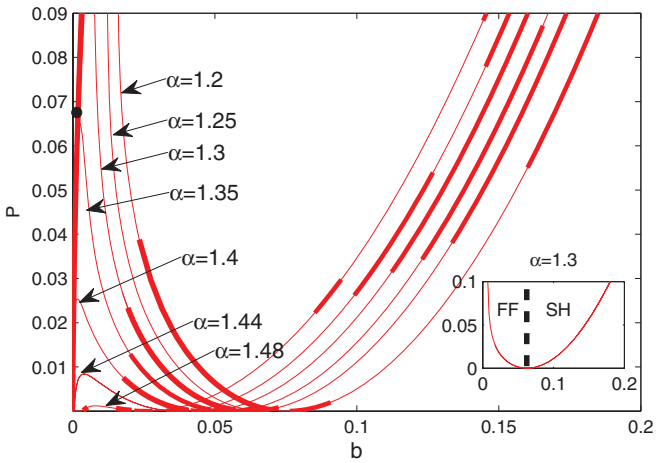

FIG. 7. (Color online) Several fundamental branches for case (iii) with different values of α. Note that the branch disappears when $\alpha \to \alpha_{cr} = 3/2$. Stable (unstable) solutions are represented by thick (thin) lines. The inset shows the regions of bifurcations from $b_{1,0}$ (FF) and $b_{2,0}$ separated by a vertical dashed line. The parameters of the structure are $V = 1/2$ and $q = q_0$ ($\alpha_{cr} = 1.5$).

$b_{2,0}$, and the branch that goes to the left is a bifurcation of $b_{1,0}$. Both branches have behaviors very similar to the branches of cases (i) and (ii).

In the numerical simulations, we observed that there may be a collision of the fundamental branch with a nonfundamental branch with two peaked solutions. Figure 8 shows the corresponding bifurcation diagrams, whereas, Fig. 9 illustrates the distribution of the intensities and the currents in a two-hump soliton solution. The intensities and the current j_2 are largely distributed far from the center of the potential, whereas, the current j_1 is localized at the defect.

In Fig. 10, one can see that, as b decreases, $|w_1(0)|^2$ decreases at the same time that the two emergent peaks become increasingly separated. The intensity $|w_2(0)|^2$ (not shown) decreases as well.

With respect to phase, we found all stable solutions that bifurcate from $b_{1,0}$ to satisfy $w_n(\xi) = \overline{w_n(-\xi)}$. This means that the peaks of the two-hump solution shown in Fig. 10 are out of phase.

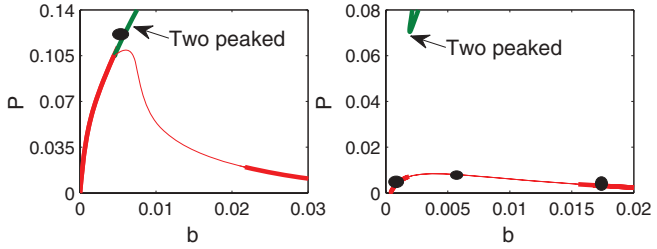

FIG. 8. (Color online) Left panel: line: shows the fundamental branch of case (iii) with $\alpha = 1.3$ near $b = 0$ and the merged two-peaked branch. Lines: thick lines are stable (unstable) solutions. Right panel: Shows a fundamental branch and a two-peaked branch with $\alpha = 1.44$ near $b = 0$. Black circles are solutions represented in Figs. 9 and 14. The parameters of the structure are $V = 1/2$ and $q = q_0$.

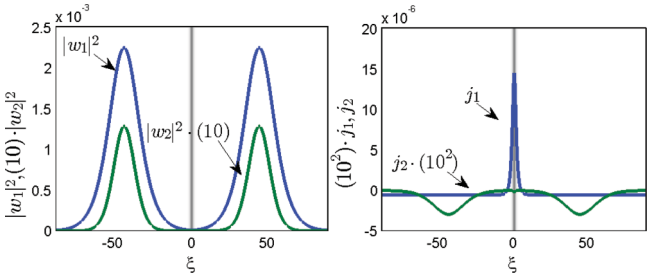

FIG. 9. (Color online) Stable double-peaked solution with $b = 0.0057$, corresponding to the black circle in the left panel of Fig. 8. The left panel shows the intensities $|w_n|^2$; the right panel shows the currents j_n. The shadowed domain shows the localized impurity $V\,\mathrm{sech}^2(\xi)$ (darker areas represent higher values of the real part of the localized potential). The parameters of the structure are $V = 1/2$, $\alpha = 1.3$, and $q = q_0$.

VI. STABILITY AND DYNAMICS OF LOCALIZED SOLUTIONS

The stability was studied by direct numerical simulations of the system (1) and within the framework of eigenvalue evaluation of the eigenvalue problem, obtained from perturbations of the form

$$u_n(\xi,\zeta) = [w_n(\xi) + p_{n+}(\xi)e^{-i\lambda\zeta} + \overline{p}_{n-}(\xi)e^{i\bar{\lambda}\zeta}]e^{inb\zeta}, \quad (23)$$

with $p_{n+}(\xi)$ and $p_{n-}(\xi)$ being small perturbations. The resulting eigenvalue problem is given by

$$\begin{pmatrix} L_2 & 2w_1 & 0 & 0 \\ 2\bar{w}_1 & L_{1,\alpha} & 0 & 2w_2 \\ 0 & 0 & -\bar{L}_2 & -2\bar{w}_1 \\ 0 & -2\bar{w}_2 & -2w_1 & -\bar{L}_{1,\alpha} \end{pmatrix} \begin{pmatrix} p_{2+} \\ p_{1+} \\ p_{2-} \\ p_{1-} \end{pmatrix} = \lambda \begin{pmatrix} p_{2+} \\ p_{1+} \\ p_{2-} \\ p_{1-} \end{pmatrix}. \quad (24)$$

Whenever an eigenvalue λ with $\mathrm{Im}(\lambda) > 0$ occurs, the solution is unstable.

Let us start the stability analysis with case (i). Then, the branches have two stable regions, one close to $b_{1,0}$ and the other close to $b = 0$ as shown in Fig. 1. It was found numerically

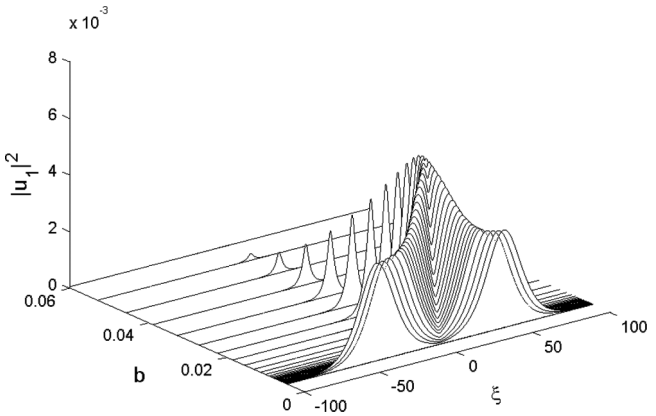

FIG. 10. The intensity profiles $|w_1|^2$ of solutions, pertaining to the fundamental branch of case (iii) bifurcating from $b_{1,0} = 0.063$ at different b's illustrating the transition of a single-peaked profile into a double-peaked one. The local minimum occurs exactly at $\xi = 0$. The parameters of the structure are $V = 1/2$, $\alpha = 1.3$, and $q = q_0$.

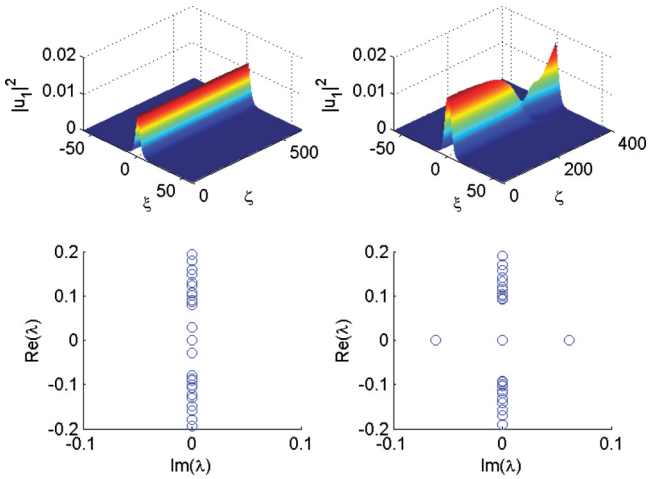

FIG. 11. (Color online) Upper left panel: the evolution of a stable solution with $b = 0.076$ and upper right panel: an unstable solution with $b = 0.09$ of the fundamental branch of case (i). The corresponding eigenvalues of the linear stability analysis are given in the lower panels. The parameters of the structure are $V = 1/2$, $q = 0$, and $\alpha = 0.9$.

that only low amplitude solutions are stable. The instability is produced by pairs of purely imaginary eigenvalues λ, see Fig. 11, showing the eigenvalues and the typical evolution of the soliton, resulting in its rapid decay.

For case (ii), we investigated the stability and found that all the solutions were stable if $\alpha \lessapprox 0.9$, for $\alpha \gtrapprox 0.9$, some parts of the bifurcation curve became unstable, see Fig. 12. In Fig. 12, one can see that the unstable part of the bifurcation curve becomes larger when α increases, but the stable solutions survive even for $\alpha \gg \alpha_{cr}$. The linear stability analysis shows that the instability arises from quartets of complex eigenvalues (see Fig. 13).

Finally, we discuss case (iii). We found that, with respect to stability, the behavior is similar to cases (i) and (ii). For values $b > b_{1,0}$, i.e., bifurcations of $b_{2,0}$, the stability behaves, such as in case (ii) with the appearance of instability intervals that increase in length as α increases. The region $b < b_{1,0}$ has solutions that bifurcate from $b_{1,0}$. There is always a stable region adjacent to $b_{1,0}$ and another stable region close to $b = 0$. The instability, when observed, was due to a quartet of complex eigenvalues of the stability matrix contained in the region $b > b_{1,0}$ and two purely imaginary eigenvalues in the region contained in $b < b_{1,0}$ (see the middle panel of Fig. 14). We observed that there were stable solutions in the region

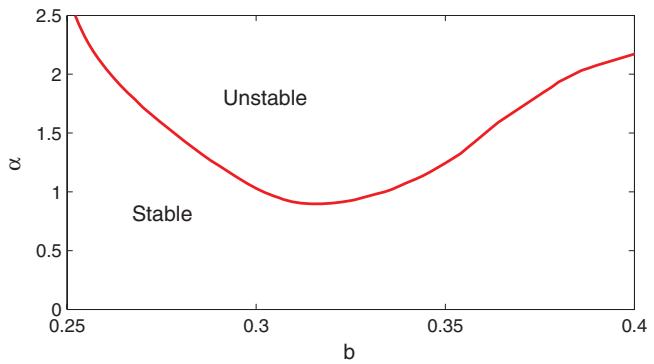

FIG. 12. (Color online) The panel shows the maximal value of α for which a fundamental branch solution is stable as a function of b. The branch bifurcates from $b_{2,0}$. The parameters of the structure are $V = 1/2$ and $q = 0$.

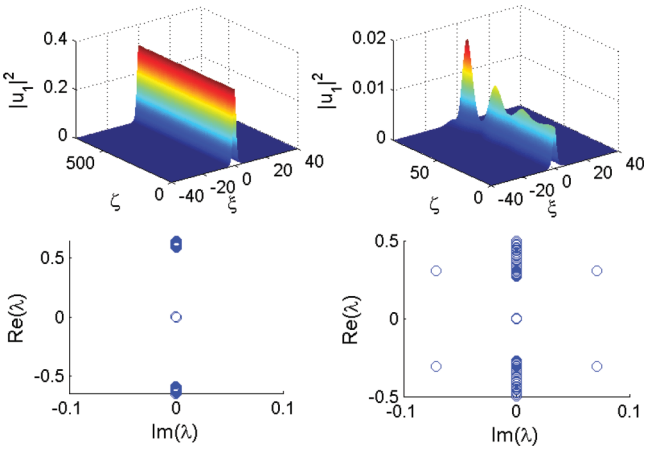

FIG. 13. (Color online) Upper left panel: the evolution of a stable solution with $b = 0.6$ and upper right panel: an unstable solution with $b = 0.27$ of the fundamental branch of case (ii) that bifurcates from $b_{2,0}$. Both solutions were perturbed by 10% of amplitude random noise. The corresponding eigenvalues of the linear stability matrix are given in the lower panels. Both solutions are marked by black circles in Fig. 5. The parameters of the structure are $V = 1/2$, $q = 0$, and $\alpha = 2$.

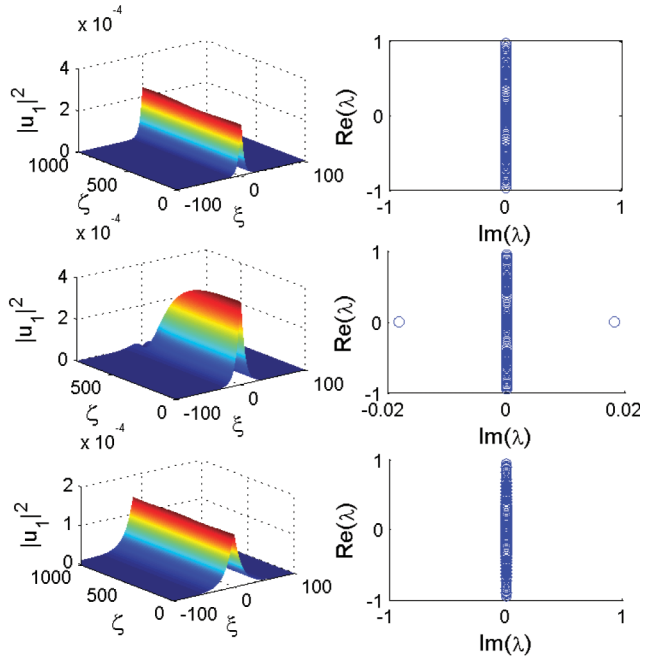

FIG. 14. (Color online) Left panels: Propagation of 10% of amplitude perturbations of solutions marked by black circles in the lower panel of Fig. 8, corresponding to case (iii). The upper left panel has $b = 0.0172$, the middle left panel has $b = 0.0072$, and the lower left panel has $b = 0.0017$. Right panels are the respective eigenvalues of the linear problem. Parameters of the structure are $V = 1/2$, $\alpha = 1.45$, and $q = q_0$.

where the fundamental branch, bifurcating from $b_{1,0}$, merged with a two-peaked branch.

VII. CONCLUSION

To summarize, we showed the existence of solitons in quadratic nonlinear media with localized $\mathcal{PT}$-symmetric modulations of linear refractive index. The families of stable one- and two-hump solitons were found. The properties of nonlinear modes bifurcating from a linear limit of small fundamental harmonic field were investigated. It was shown that the fundamental branch had a maximum in a power. This maximum was decreasing with the strength of the imaginary part of the refractive index α. For the case when both harmonics were on the same order, the scenarios of bifurcations of different branches of solutions on the propagation constant b were investigated. It was shown that modes bifurcating from the linear mode of the second harmonic can exist, even above the $\mathcal{PT}$-symmetry-breaking threshold. We found that the fundamental branch bifurcating from the linear limit can undergo a secondary bifurcation colliding with a branch of two-hump soliton solutions.

For nonlinear modes, having no linear limit, i.e., $|u_2| \sim O(1)$, different branches of solutions, in dependence on the parameters b and the phase mismatch q, had been investigated. The stability intervals for different values of parameters b and α were obtained. The examples of dynamics and excitations of solitons by numerical simulations of the full $\chi^{(2)}$ system of equations with the $\mathcal{PT}$-symmetric potential were confirmed theoretical predictions.

ACKNOWLEDGMENTS

F.C.M. acknowledges support from the EU Alban program. V.V.K. and A.V.Y. acknowledge support from the FCT (Portugal) under Grants No. PTDC/FIS/112624/2009 and No. PEst-OE/FIS/UI0618/2011. F.K.A. acknowledges support from the FAPESP (Brazil).

[1] C. M. Bender and S. Boettcher, Phys. Rev. Lett. **80**, 5243 (1998).
[2] A. Ruschaupt, F. Delgado, and J. G. Muga, J. Phys. A **38**, L171 (2005).
[3] A. Guo, G. J. Salamo, D. Duchesne, R. Morandotti, M. Volatier-Ravat, V. Aimez, G. A. Siviloglou, and D. N. Christodoulides, Phys. Rev. Lett. **103**, 093902 (2009); C. E. Rüter, K. G. Makris, R. El-Ganainy, D. N. Christodoulides, M. Segev, and D. Kip, Nat. Phys. **6**, 192 (2010).
[4] Z. H. Musslimani, K. G. Makris, R. El-Ganainy, and D. N. Christodoulides, Phys. Rev. Lett. **100**, 030402 (2008).
[5] M. Znojil, J. Phys. A **33**, L61 (2000).
[6] Z. Ahmed, Phys. Lett. A **282**, 343 (2001).
[7] S. Hu, X. Ma, D. Lu, Z. Yang, Y. Zheng, and W. Hu, Phys. Rev. A **84**, 043818 (2011).
[8] Z. Shi, X. Jiang, X. Zhu, and H. Li, Phys. Rev. A **84**, 053855 (2011).
[9] A. Mostafazadeh, Phys. Rev. A **80**, 032711 (2009).
[10] O. Bendix, R. Fleischmann, T. Kottos, and B. Shapiro, Phys. Rev. Lett. **103**, 030402 (2009).
[11] F. K. Abdullaev, V. V. Konotop, M. Ögren, and M. P. Sørensen, Opt. Lett. **36**, 4566 (2011).
[12] H. Cartarius and G. Wunner, arXiv:1203.1885.
[13] F. K. Abdullaev, V. V. Konotop, M. Salerno, and A. V. Yulin, Phys. Rev. E **82**, 056606 (2010); F. K. Abdullaev, Y. V. Kartashov, V. V. Konotop, and D. A. Zezyulin, Phys. Rev. A **83**, 041805(R) (2011); Y. He, X. Zhu, D. Mihalache, J. Liu, and Z. Chen, *ibid.* **85**, 013831 (2012); S. Nixon, L. Ge, and J. Yang, *ibid.* **85**, 023822 (2012); V. Achilleos, P. G. Kevrekidis, D. J. Frantzeskakis, and R. Carretero-González, *ibid.* **86**, 013808 (2012); J. Zeng and Y. Lan, Phys. Rev. E **85**, 047601 (2012); S. V. Suchkov, S. V. Dmitriev, B. A. Malomed, and Y. S. Kivshar, Phys. Rev. A **85**, 033825 (2012).
[14] C. B. Clausen, J. P. Torres, and L. Torner, Phys. Lett. A **249**, 455 (1998).
[15] C. B. Clausen and L. Torner, Phys. Rev. Lett. **81**, 790 (1998).
[16] B. Midya, B. Roy, and R. Roychoudhury, Phys. Lett. A **374**, 2605 (2010).
[17] D. Landau and E. M. Lifshitz, *Quantum Mechanics: Non-Relativistic Theory* (Elsevier Science, Waltham, MA, 1958), Vol. 3.
[18] D. A. Zezyulin and V. V. Konotop, Phys. Rev. Lett. **108**, 213906 (2012).
[19] E. N. Tsoy, S. Tadjimuratov, and F. K. Abdullaev, Opt. Commun. **285**, 3441 (2012).